Materials Advances

ROYAL SOCIETY OF CHEMISTRY

PAPER

View Article Online
View Journal | View Issue

Check for updates

Cite this: *Mater. Adv.*, 2022, 3, 1240

Tuning the switching pressure in square lattice coordination networks by metal cation substitution†

Shi-Qiang Wang, Shaza Darwish, Debobroto Sensharma and Michael J. Zaworotko *

Received 31st August 2021,
Accepted 8th December 2021

DOI: 10.1039/d1ma00785h

rsc.li/materials-advances

Coordination networks that undergo guest-induced switching between "closed" nonporous and "open" porous phases are of increasing interest as the resulting stepped sorption isotherms can offer exceptional working capacities for gas storage applications. For practical utility, the gate ad/desorption pressures (P_{ga}/P_{gd}) must lie between the storage (P_{st}) and delivery (P_{de}) pressures and there must be fast switching kinetics. Herein we study the effect of metal cation substitution on the switching pressure of a family of square lattice coordination networks $[M(4,4'\text{-bipyridine})_2(NCS)]_n$ (**sql-1-M-NCS**, M = Fe, Co and Ni) with respect to CO_2 sorption. The Clausius–Clapeyron equation was used to correlate P_{ga}/P_{gd} and temperature. At 298 K, P_{ga}/P_{gd} values were found to vary from 31.6/26.7 bar (M = Fe) to 26.7/20.9 bar (M = Co) and 18.5/14.6 bar (M = Ni). The switching event occurs within 10 minutes as verified by dynamic CO_2 sorption tests. In addition, *in situ* synchrotron PXRD and molecular simulations provided structural insight into the observed switching event, which we attribute to layer expansion of **sql-1-M-NCS** *via* intercalation and inclusion of CO_2 molecules. This study could pave the way for rational control over P_{ga}/P_{gd} in switching adsorbent layered materials and enhance their potential utility in gas storage applications.

Open Access Article. Published on 10 December 2021. Downloaded on 4/23/2024 8:59:29 PM.
This article is licensed under a Creative Commons Attribution-NonCommercial 3.0 Unported Licence.

Introduction

New approaches to gas storage/delivery are needed in the "age of gas" to address the large energy footprint associated with existing technologies such as compressed or liquefied gas storage.[1] Whereas physisorption holds promise for greatly improving the energy efficiency of industrial gas storage, it does not yet meet the prerequisites for practical deployment such as adsorbed natural gas (ANG) storage.[2] This is at least partly because rigid physisorbents such as zeolites tend to suffer from inappropriate sorption isotherms (Langmuir or type I[3]), resulting in lower working capacity than the saturation uptake (Scheme 1a).[4]

Metal–organic materials (MOMs),[5,6] such as metal–organic frameworks (MOFs),[7,8] or porous coordination polymers/networks (PCPs/PCNs),[9–12] have attracted attention from academic and industrial researchers thanks to their potential utility in the areas as broad as storage, separation and catalysis.[13,14] A prominent feature of MOMs is their inherent modularity which enables fine tuning of structures through crystal engineering or reticular chemistry.[15,16] However, although *ca.* 1 00 000 MOMs have been deposited in the MOF subset of the Cambridge Structural Database (CSD),[17] most are rigid physisorbents that

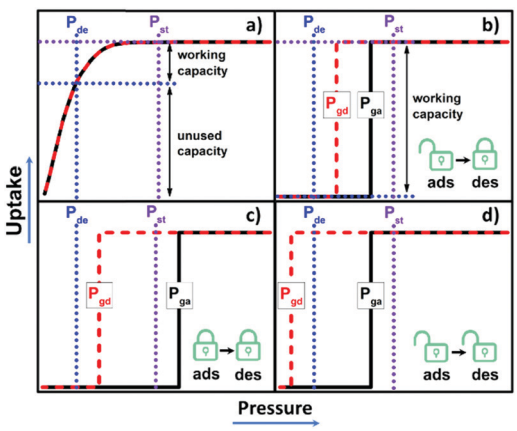

Scheme 1 Comparison of different types of gas sorption isotherms. (a) type I; (b) type F-IV ($P_{de} < P_{gd} < P_{ga} < P_{st}$); (c) type F-IV ($P_{de} < P_{gd} < P_{st} < P_{ga}$) and (d) type F-IV ($P_{gd} < P_{de} < P_{ga} < P_{st}$). Black solid line: adsorption; red dash line: desorption; P_{ga}: gate adsorption pressure; P_{gd}: gate desorption pressure; P_{de}: delivery pressure; P_{st}: storage pressure; ads: adsorption; des: desorption.

Department of Chemical Sciences and Bernal Institute, University of Limerick, Limerick V94 T9PX, Republic of Ireland. E-mail: Michael.Zaworotko@ul.ie

† Electronic supplementary information (ESI) available: Synchrotron PXRD patterns, water vapour sorption isotherms, TGA curves, Clausius–Clapeyron calculations, *etc.* CCDC 2106581–2106583. For ESI and crystallographic data in CIF or other electronic format see DOI: 10.1039/d1ma00785h

© 2022 The Author(s). Published by the Royal Society of Chemistry

Open Access Article. Published on 10 December 2021. Downloaded on 4/23/2024 8:59:29 PM. This article is licensed under a Creative Commons Attribution-NonCommercial 3.0 Unported Licence.

exhibit the aforementioned type I sorption isotherms. In contrast, flexible MOMs (FMOMs) or soft porous crystals (SPCs) can undergo guest-induced switching between nonporous and porous phases and exhibit perhaps the most desirable isotherm type, a stepped or type F-IV isotherm.[18–20] The optimal type F-IV isotherm would offer gate adsorption (P_{ga}) and desorption (P_{gd}) pressures that lie between the storage (P_{st}) and delivery (P_{de}) pressures to enable high working capacity (Scheme 1b). There is little margin for error, however, as FMOMs that remain closed during adsorption ($P_{ga} > P_{st}$, Scheme 1c) or open during desorption ($P_{gd} < P_{de}$, Scheme 1d) will offer negligible working capacity. Furthermore, gas storage criteria for P_{st} and P_{de} could vary significantly in different circumstances. The ability to fine-tune the switching pressures in FMOMs is thus important to enable the development of bespoke adsorbent materials for gas storage/delivery. Thus far, to our knowledge, only a relatively small subset of FMOMs feature type F-IV isotherms and even fewer have been subjected to systematic studies that address how to control their switching pressures.[21]

Crystal-engineering approaches can be exploited to tailor structures, compositions and, therefore, properties of MOMs.[22] In the context of FMOMs, ligand "linker" or metal "node" substitution can be used to modulate flexibility.[23–26] Ligand functionalization was used to adjust the switching of parent sorbents such as MIL-53(Fe) and [Co(bdp)].[27–29] Regarding ligand substitution, we recently reported a family of two-fold interpenetrated FMOMs, X-pcu-*n*-Zn (n = 5–8), which exhibited pronounced switching behavior with comparable uptakes but different switching pressures.[30,31] Considerable attention has been paid to exploiting metal cation substitution to modulate FMOM platforms, however, it can be a challenge to retain the type F-IV sorption profile.[32–37] For example, MIL-53(Cr or Al) were found to exhibit type F-I isotherms for CO_2 sorption,[32] while MIL-53(Fe or Sc) featured type F-IV isotherms.[33,34] In addition, the Co and Fe variants of [M(bdp)] exhibited type F-IV isotherms,[4] but their Zn and Ni analogues showed type I isotherms.[35] The pillared-layer coordination networks, DUT-8(M), exhibited type F-IV (DUT-8(Ni)), type F-I (DUT-8(Co)) or type I (DUT-8(Cu)) isotherms upon CO_2 sorption.[36] Even though the zeolitic imidazolate frameworks [M(bim)$_2$] (M = Co, Zn and Cd) retained their switching nature, there a significant pre-step was observed in the Co and Zn variants.[37] Herein we address the use of metal cation substitution to tune the switching pressure in a family of three square lattice (**sql**) coordination networks [M(bpy)$_2$(NCS)$_2$]$_n$, **sql-1-M-NCS** (1 = bpy = 4,4′-bipyridine, M = Fe, Co and Ni).

Square lattice (**sql**) coordination networks account for nearly half of reported 2D coordination networks (CNs).[38] **sql** CNs with general formula [**M**(**L**)$_2$(**A**)$_2$] can be readily formed by self-assembly of octahedral metal ions (**M**), axial counter anions (**A**) and linear linker ligands (**L**).[39] The prototypal non-interpenetrated **sql** CN, [Cd(bpy)$_2$(NO$_3$)$_2$]$_n$, was reported by Fujita's group in 1994.[40] This seminal work was followed by a series of studies that focused more upon the structural features of such networks rather than sorption properties until [Cu(bpy)$_2$(BF$_4$)$_2$] (ELM-11) was investigated.[41,42] ELM-11 was found to exhibit switching when exposed to gases such as CO_2, C_2H_2 and *n*-butane.[43–47] Its metal cation substituted analogue, [Ni(bpy)$_2$(BF$_4$)$_2$] (ELM-31), also exhibits a type F-IV isotherm upon CO_2 sorption but with different uptake and switching pressure.[48] Nevertheless, the metal substitution strategy has not yet been fully exploited in the ELM-11 family.

Recently, our group reported the sorption properties of a previously known **sql** CN [Co(bpy)$_2$(NCS)$_2$],[49] **sql-1-*Co*-NCS**,[50,51] which is closely related to the ELM family.[43,44] The 195 K CO_2 sorption isotherm of **sql-1-*Co*-NCS** was observed to be type F-IV.[50] High-pressure CO_2 sorption at different temperatures exhibited type F-IV sorption profiles and the temperature *vs* switching pressure obeyed the Clausius–Clapeyron equation. Crystallographic studies revealed that the interlayer distance in the closed phase (4.5 Å) increased in the CO_2 loaded phase (5.4 Å), although the location of CO_2 molecules was not determined.[50] In this contribution, we report the Fe and Ni analogues of **sql-1-*Co*-NCS** and their CO_2 sorption profiles and switching kinetics.

Results and discussion

sql-1-M-NCS (M = Fe and Ni) were synthesized in powder form (rod shape, 0.5–2 μm, Fig. S14, ESI†) by heating their precursors {[M(bpy)(NCS)$_2$(H$_2$O)$_2$]·bpy}$_n$ at 50 °C *in vacuo*. These precursors were prepared by a water slurry method. The crystal structures of **sql-1-*Co*-NCS** and **sql-1-Ni-NCS** were previously determined by single-crystal X-ray diffraction[50,52] and we determined the crystal structure of **sql-1-Fe-NCS** herein by refinement of synchrotron PXRD data (Fig. S1 and S3a, ESI†). The three **sql-1-M-NCS** CNs are comprised of M(II) cations coordinated to four equatorial bpy ligands and two axial NCS$^-$ ligands and they are isostructural. Their synchrotron PXRD patterns match well (Fig. S1, ESI†). The effective cavity sizes (7.5 Å × 7.5 Å) and interlayer distances (4.5 Å) are also equivalent, although there are minor differences in the torsion angle of the bpy linker ligands (54.3°–54.7°) and the M–M–M (75.3°–76.4°) and M–N–CS (169.5°–170.9°) angles (Fig. 1). Terminal NCS ligands interdigitate adjacent layers (Fig. 1d–f) and block the cavities.

Although the cavity size and interlayer distance of **sql-1-M-NCS** are comparable to those of ELM-11, the hydrophilicity of **sql-1-M-NCS** towards humidity is mitigated thanks to utilisation of the relatively hydrophobic NCS$^-$ anion (Fig. S4, ESI†). Thermogravimetric analysis (TGA) revealed that **sql-1-Ni-NCS** exhibits better thermal stability (*ca.* 180 °C) than its Fe and Co analogues (*ca.* 150 °C) (Fig. S5, ESI†), which follows the empirical Irving–Williams series.[53] 195 K CO_2 sorption studies revealed that **sql-1-M-NCS** CNs exhibit the same saturation uptake (*ca.* 138 cm^{-3} g^{-1}), equivalent to three CO_2 molecules per formula unit (denoted as **sql-1-M-NCS**·**3CO$_2$**), but with distinct P_{ga}/P_{gd} values: Fe (15/12 kPa) > Co (10/8 kPa) > Ni (4/3.5 kPa) (Fig. 2). Unlike ELM-11 which exhibits multi-step CO_2 sorption isotherms at 195 K,[54,55] **sql-1-M-NCS** registered single-step sorption isotherms although **sql-1-Fe-NCS** had a small sub-step with 17 cm^{-3} g^{-1} uptake between 11 and 15 kPa.

Open Access Article. Published on 10 December 2021. Downloaded on 4/23/2024 8:59:29 PM.
This article is licensed under a Creative Commons Attribution-NonCommercial 3.0 Unported Licence.

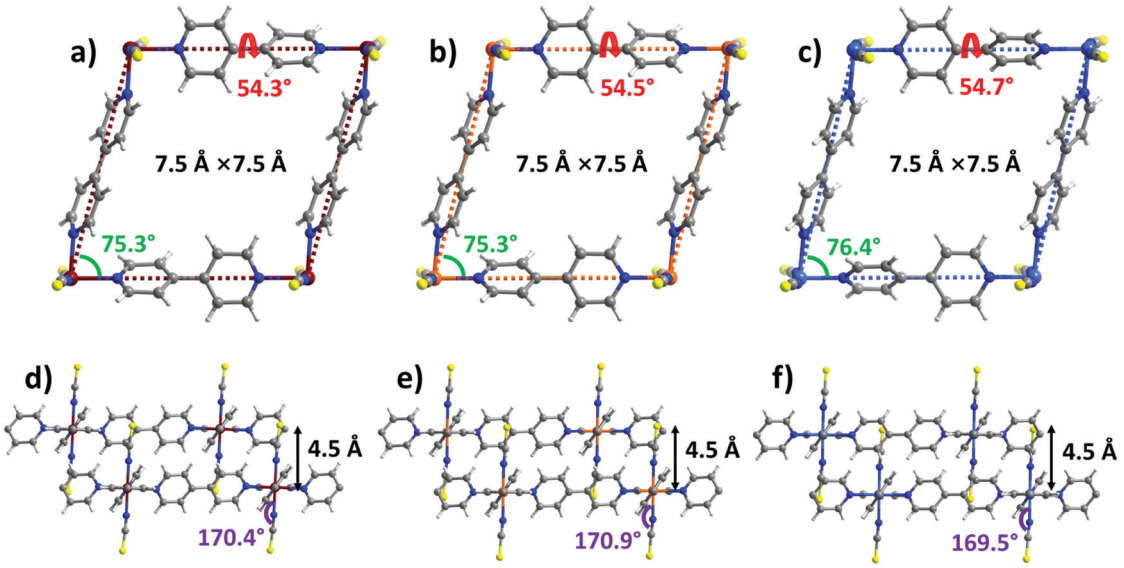

Fig. 1 Comparison of the crystal structures of **sql-1-M-NCS**. (a and d) M = Fe; (b and e) M = Co; (c and f) M = Ni.

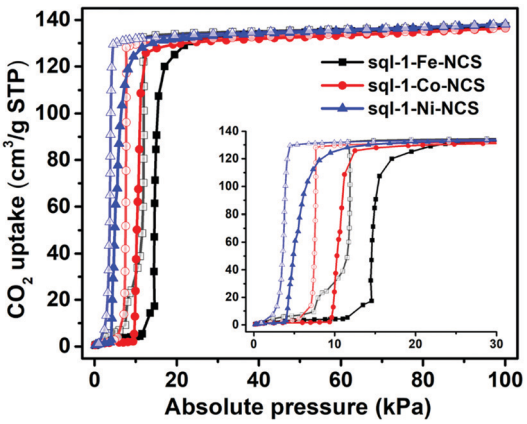

Fig. 2 CO_2 sorption isotherms for **sql-1-M-NCS** (M = Fe, Co, and Ni) at 195 K. The solid and open symbols represent adsorption and desorption branches, respectively.

We next collected high-pressure (up to 38 bar) CO_2 sorption isotherms on **sql-1-M-NCS** (M = Fe and Ni) between 273 and 298 K (5 K intervals) as previously conducted for **sql-1-*Co*-NCS** (Fig. 3a, b and Fig. S6, ESI†). The P_{ga}/P_{gd} values for **sql-1-Fe-NCS** were 12.5/10.5, 15.2/12.8, 18.5/15.5, 22.3/18.7, 26.6/22.6 and 31.6/26.7 bar from 273 to 298 K, respectively. In contrast, **sql-1-Ni-NCS** was found to offer lower P_{ga}/P_{gd} values: 6.5/5.1, 8.1/6.4, 10.1/7.9, 12.5/9.8, 15.2/11.9 and 18.5/14.5 bar from 273 to 298 K, respectively. The CO_2 sorption isotherms of **sql-1-M-NCS** (M = Fe and Ni) revealed a relationship between the P_{ga}/P_{gd} and temperature which obeys the Clausius–Clapeyron equation $d\ln P/(d(1/T)) = (\pm)\Delta H/R$ (Fig. 3c, d and Fig. S7, ESI†). The phase transition enthalpies ΔH (the signs of ΔH are negative/positive for adsorption/desorption, respectively, absolute values are used hereafter) were calculated to be *ca.* 25.2 and 28.4 kJ mol^{-1} for **sql-1-Fe-NCS** and **sql-1-Ni-NCS**, respectively, 1.0 kJ mol^{-1} lower and 2.2 kJ mol^{-1} higher than that of **sql-1-*Co*-NCS** (26.2 kJ mol^{-1}).[50]

One advantage of switching CNs is the switching pressure can be calculated at a given temperature once ΔH in the Clausius–Clapeyron equation has been determined.[47,50] We thus plotted calculated switching pressure *vs* temperature from 195 to 298 K for **sql-1-M-NCS** (M = Fe, Co and Ni) (Fig. 3e, f and Fig. S8, Table S1, ESI†). The P_{ga} and P_{gd} were thereby tuned by the metal centers: P_{ga}/P_{gd} (Fe) > P_{ga}/P_{gd} (Co) > P_{ga}/P_{gd} (Ni). Since the switching pressure is exponentially correlated to the temperature, it increases substantially at elevated temperature. For example, at 298 K, the P_{ga}/P_{gd} were calculated to be 31.6/26.7, 26.7/20.9, and 18.5/14.6 bar when M = Fe, Co and Ni, respectively, two orders of magnitude higher than at 195 K. The magnitude of the hysteresis between P_{ga} and P_{gd} was also affected by temperature (Fig. S8, ESI†). The hysteresis gaps were found to be 4.9 (Fe), 5.8 (Co) and 3.9 (Ni) bar at 298 K, 163, 290, and 780 times their values (3.0, 2.0, and 0.5 kPa) at 195 K. The hysteresis in **sql-1-M-NCS** suggests that CO_2 can be stored at lower pressure (between P_{gd} and P_{ga}) than the charging pressure (P_{ga} or above).

When compared to other switching CNs which exhibit wide ranges of CO_2 uptakes (40–590 cm^{-3} g^{-1}) and switching pressures (1.3–75 kPa) at 195 K (Table S2 and Fig. S9a, ESI†),[21] **sql-1-M-NCS** exhibit moderate uptakes and relatively low switching pressures. At elevated temperature (*e.g.* 298 K), **sql-1-M-NCS** retained almost the same uptake, whereas some benchmark switching CNs like DUT-8(Ni) and X-pcu-*n*-Zn tend to exhibit lower or even negligible CO_2 uptakes (Table S2 and Fig. S9b, ESI†),[31,36] due to P_{ga} values (*e.g.* >35 bar) that are beyond the maximum testing pressures. The prototypical switching **sql** CN, ELM-11, was observed to exhibit 80 and 173 cm^{-3} g^{-1} of CO_2 uptake at the first ($P_{ga}1$ = 0.65 bar) and second steps ($P_{ga}2$ = 19 bar) at 298 K.[54] The distinct differences between ELM-11 and **sql-1-M-NCS** demonstrate the feasibility of tuning the switching pressure and even the uptake in families of **sql-1** CNs.

The sorption kinetics of sorbents is also relevant to their storage and separation performance,[56–58] especially for FMOMs

© 2022 The Author(s). Published by the Royal Society of Chemistry

Open Access Article. Published on 10 December 2021. Downloaded on 4/23/2024 8:59:29 PM.
This article is licensed under a Creative Commons Attribution-NonCommercial 3.0 Unported Licence.

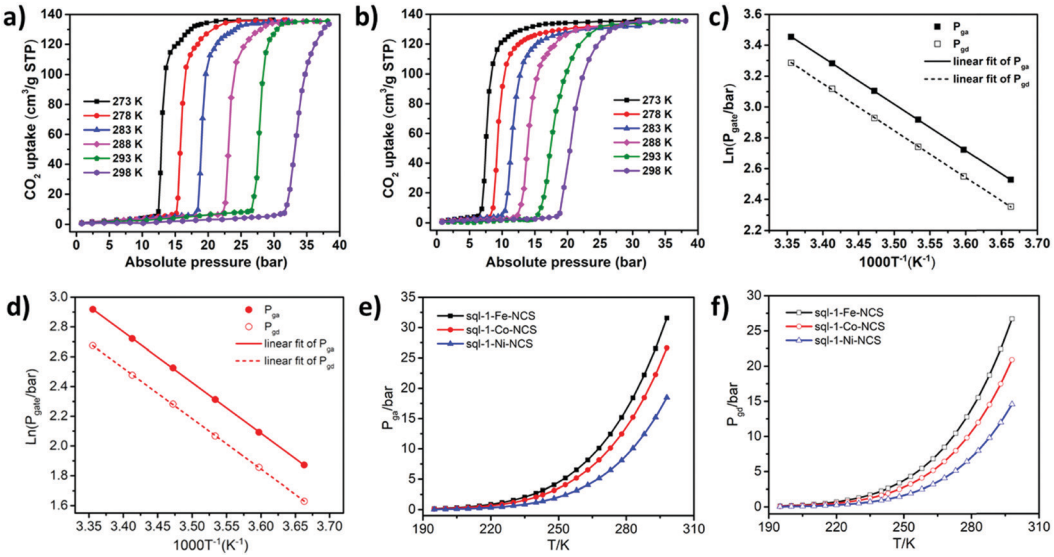

Fig. 3 High-pressure CO_2 sorption isotherms of (a) **sql-1-Fe-NCS** and (b) **sql-1-Ni-NCS**. The linear fit of gate sorption pressure (LnP) and temperature (1000 T^{-1}) using the Clausius–Clapeyron equation for (c) **sql-1-Fe-NCS** and (d) **sql-1-Ni-NCS**. (e) Calculated P_{ga} and (f) P_{gd} for **sql-1-M-NCS** (M = Fe, Co, and Ni).

featuring structural transitions that might control the kinetics.[51,59–61] We conducted dynamic CO_2 sorption studies on **sql-1-M-NCS** gravimetrically at 288 K and 1–36 bar. The CO_2 pressure was elevated/reduced constantly with a maximum rate of 2.5 bar min^{-1} for adsorption/desorption process. It was observed that **sql-1-M-NCS** started adsorbing/desorbing CO_2 at 11.5/7.8, 10.0/9.5 and 7.5/10.8 min (equivalent to 23.9/18.0, 20.0/13.9 and 13.5/10.7 bar) for M = Fe, Co and Ni, respectively (Fig. 4). It is consistent with the P_{ga}/P_{gd} values (22.2/18.7, 18.5/14.5 and 12.4/9.8 bar) calculated from the Clausius–Clapeyron equation at 288 K. We determined that it took 7.5/5, 6/6 and 5/7.5 min to reach full loading/unloading for **sql-1-M-NCS** (M = Fe, Co, and Ni, respectively), indicating *ca.* 12.5 min for a sorption cycle and 22 cm^{-3} g^{-1} min^{-1} for the average sorption rate. It was reported that ELM-11 reaches full loading of CH_4 (*ca.* 80 cm^{-3} g^{-1}) in 10 min at 303 K.[43] Such sorption kinetics of **sql** CNs is comparable or even superior to some rigid sorbents.[56,62]

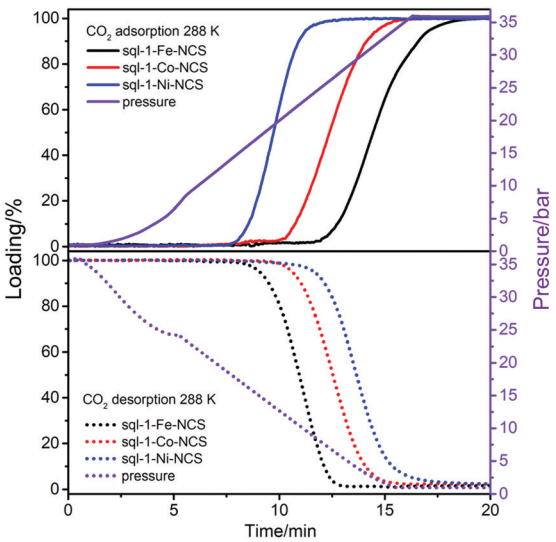

Fig. 4 Kinetics of CO_2 adsorption (top) and desorption (bottom) for **sql-1-M-NCS** (M = Fe, Co and Ni) at 288 K.

To better understand the switching mechanism of **sql-1-M-NCS**, *in situ* CO_2 loaded synchrotron PXRD experiments (Fig. S2, ESI†) and molecular simulations were conducted. As revealed by Fig. 5, the cavity size of **sql-1-M-NCS·3CO$_2$** remains unchanged compared to that of **sql-1-M-NCS**, however, the cavity geometry deforms from a rhombus in the closed phase to a square in the open phase accompanied by an interlayer distance increase from 4.5 to 5.4 Å. Such intra-network and inter-network deformations induced by guest molecules are quite common amongst switching and flexible CNs.[21,63,64] In addition, the bpy ligand twists by 10.3° (Fe), 9.6° (Co), and 8.9° (Ni) to accommodate the CO_2 molecules which occupy the interlayer and cavity voids as visualised by molecular simulations. It also reveals that $[CO_2]_3$ cluster units are formed (C···O distance: 2.755–3.265 Å) in the cavities of **sql-1-M-NCS·3CO$_2$** and propagate along *a* axis (Fig. S10–S12, ESI†). Each strand of $\{[CO_2]_3\}_n$ is constrained in half of the cavity thanks to the ABAB stack mode of layers. Notably, the M–N–CS angles are compressed to 144.9° (Fe), 156.1° (Co) and 162.1° (Ni) in the open phases, corresponding to a change of 25.5°, 14.8°, and 7.4° from those in the closed phases, respectively. Overall, transformations between sql-1-M-NCS and sql-1-M-NCS·3CO2 followed the trend P_{ga} (Fe) > P_{ga} (Co) > P_{ga} (Ni), corresponding enthalpy changes being 25.2 (Fe) < 26.2 (Ni) < 28.4 (Ni) kJ mol^{-1} (exothermic or endothermic for adsorption or desorption, respectively). Such trends could be attributable ligand twisting, metal coordination sphere distortion, layered net expansion

Open Access Article. Published on 10 December 2021. Downloaded on 4/23/2024 8:59:29 PM.
This article is licensed under a Creative Commons Attribution-NonCommercial 3.0 Unported Licence.

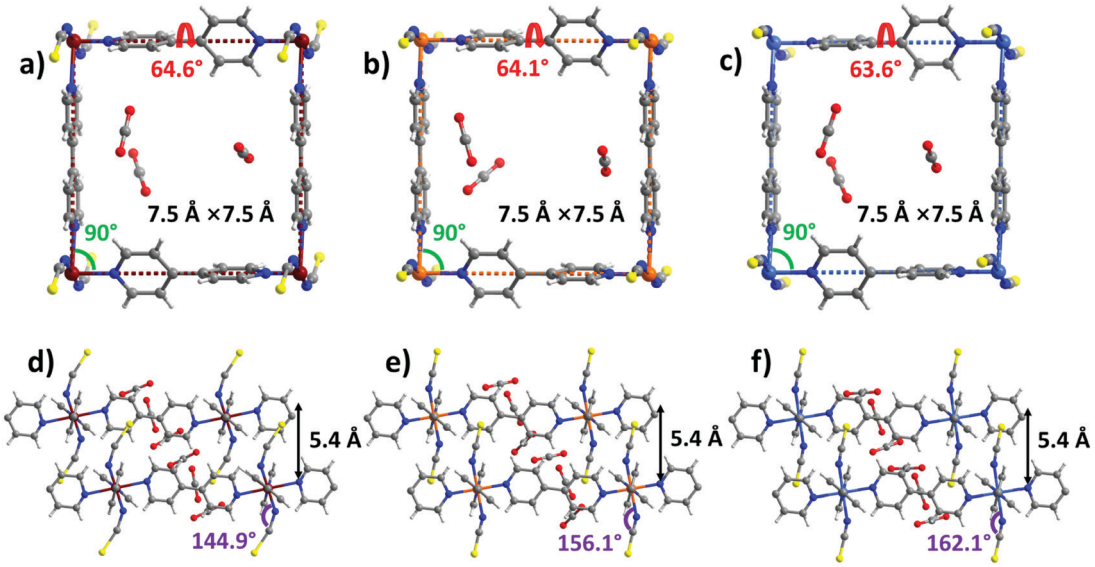

Fig. 5 Comparison of the crystal structures of **sql-1-M-NCS·3CO$_2$**. (a and d) M = Fe; (b and e) M = Co; (c and f) M = Ni.

and/or sorbate/sorbent interactions. The isostructural nature within each set of three phases suggests that, as for many trends in d-block metals, electronic configurations (d^6, d^7 and d^8), which influence metal–ligand bonding and electrostatics, are behind the observed trends. A similar situation was reported for metal substituted variants of ZIF-7.[37]

Conclusions

In conclusion, we report herein the switching behavior of three **sql-1-M-NCS** CNs through CO_2 sorption under equilibrium and dynamic conditions. Although metal cation substitution is a simple crystal engineering strategy for modulating the properties of MOMs, to our knowledge this is the first example of switching CNs that retain stepped sorption isotherms across three metal nodes. Crystallographic and modelling studies reveal that the metal centers affect the conformations in **sql-1-M-NCS·3CO$_2$**, which in turn reflect the switching pressure required for the structural transition. While several metrics such as kinetics, hydrophobicity, and strong stability to regeneration, as exemplified by **sql-1-*Co*-NCS**,[50] are favorable in **sql-1-M-NCS**, their working capacity, a key metric for gas storage, could be improved. This is particularly the case for ANG, for which the latest DOE target is 700 cm^{-3} g^{-1} or 263 cm^{-3} cm^{-3}.[65] Unfortunately, even the "softest" **sql-1-M-NCS** (*i.e.* **sql-1-Ni-NCS**) exhibited negligible CH_4 uptake below 60 bar at 298 K (Fig. S13, ESI†). This is most likely because CH_4 interacts weakly with host frameworks compared to CO_2. In contrast, stronger binding aromatics such as xylenes adsorb *ca.* 87 wt% in **sql-1-*Co*-NCS** and we recently reported that ELM-11 (**sql-1-Cu-BF$_4$**) adsorbs up to 245 cm^{-3} g^{-1} of C_2H_2 *via* four sorption steps.[47,51] The findings herein suggest that adsorbate-dependent uptake and switching pressure in families of **sql** CNs are likely to be a common feature of such switching CNs and the study of other hydrocarbons will be conducted.

Experimental section

Synthesis of square lattice (sql) coordination networks

$[Fe(bpy)_2(NCS)_2]_n$ (**sql-1-Fe-NCS**) was prepared by a water slurry method. $FeSO_4·7H_2O$ (10 mmol, 2.78 g), NaSCN (20 mmol, 1.62 g) and 4,4′-bipyridine (20 mmol, 3.12 g) were added to 50 mL water in a 100 mL bottle. The slurry was stirred continuously for 3 h at room temperature to form the precursor $\{[Fe(bpy)(NCS)_2(H_2O)_2]$ bpy$\}_n$ which was then filtered, washed with water and air-dried (yield ~95%). The precursor powder was activated at 50 °C *in vacuo* for 5 h to transform to the **sql** coordination network: **sql-1-Fe-NCS**.

$[Ni(bpy)_2(NCS)_2]_n$ (**sql-1-Ni-NCS**) was prepared by the same method as described above except that the metal salt $FeSO_4·7H_2O$ was replaced by $NiSO_4·6H_2O$ (10 mmol, 2.63 g).

Synchrotron powder X-ray diffraction

Synchrotron PXRD data was obtained from beamline I11 at the Diamond Light Source (λ = 0.82455(2) Å and zero point = −0.01826(1)°). Powder sample sealed in a Φ = 0.5 mm capillary tube was measured at 195 K under vacuum using positional scanning detector (PSD). After that, CO_2 (195 K, 1 bar) was filled into the capillary tube and powder X-ray data was collected until sample stabilized. The data was used for structure solution and refinement of **sql-1-Fe-NCS** and **sql-1-M-NCS 3CO$_2$** (M = Fe and Ni). Analysis of the powder data was carried out in TOPAS Academic and FullProf. The previously reported crystal structures of **sql-1-*Co*-NCS** and **sql-1-*Co*-NCS 3CO$_2$** were used as starting templates.[50] Lattice parameters were determined using the Pawley method. The CO_2 location was not determined by synchrotron PXRD refinement while it was modelled by molecular simulation (see simulation section below). Crystallographic data (CCDC number: 2106581–2106583) is summarized in Table S3 (ESI†) and comparative patterns for the observed and calculated intensities including their differences are presented in Fig. S3 (ESI†).

© 2022 The Author(s). Published by the Royal Society of Chemistry

Open Access Article. Published on 10 December 2021. Downloaded on 4/23/2024 8:59:29 PM. This article is licensed under a Creative Commons Attribution-NonCommercial 3.0 Unported Licence.

Density functional theory (DFT) calculations

All periodic DFT calculations were carried out using the Castep as implemented in the Materials Studio package. Vanderbilt-type ultrasoft pseudopotentials and the generalized gradient approximation (GGA) with the Perdew–Burke–Ernzerhof (PBE) exchange correlation were used for all structure calculations. A semi-empirical dispersion correction was included in the calculation to take the van der Waals interactions into account. A cutoff energy of 544 eV and a $2 \times 3 \times 2$ *k*-point mesh (generated using the Monkhorst–Pack scheme) were found to be sufficient for total energy to converge within 0.01 meV atom^{-1}. The starting structures (**sql-1-M-NCS·3CO$_2$**) were obtained from the synchrotron PXRD refinement as described above. Three CO_2 molecules per formula unit were added into each structure based on CO_2 sorption studies and were set flexible to allow the optimization of their binding sites. All the simulations on the structures were conducted in *P1* space group.

Thermogravimetric analysis (TGA)

TGA for all the compounds were carried out under N_2 atmosphere in a TA instruments Q50 thermal analyzer between room temperature and 300 °C with a constant heating rate of 10 °C min^{-1}.

Scanning electron microscopy (SEM)

SEM analysis was performed using an SU 70 Hitachi instrument. The samples were sputter-coated with gold (20 mA, 90 s) prior to imaging.

Low pressure CO_2 adsorption

Low pressure CO_2 adsorption experiments (up to 1 bar) of **sql-1-M-NCS** (M = Fe and Ni) were conducted on the Micromeritics TriStar II PLUS 3030 instrument at 195 K which was maintained by a 4 L Dewar flask filled with the mixture of acetone and dry ice. High-purity CO_2 was used as received from BOC Gases Ireland, CP grade (99.995%).

High pressure CO_2 adsorption

High pressure CO_2 isotherms of **sql-1-M-NCS** (M = Fe and Ni) were collected on a Micromeritics HPVA II-100 instrument at different temperatures (273–298 K). The activated sample (*ca.* 300 mg) was further degassed *in situ* for 1 hour before the measurements. Free spaces were determined at 0.7 bar Helium (He) and 25 °C. A background correction was performed by subtracting the adsorption of the empty sample cell from the obtained isotherms.

Water vapor sorption

Water vapor sorption measurements were conducted using a Surface Measurement Systems DVS Vacuum at 298 K. Samples of ELM-11 (purchased from TCI) and **sql-1-M-NCS** (M = Fe and Ni) were further degassed under vacuum (1×10^{-4} Torr) *in situ* and stepwise increase in relative pressure from 0 to 90% were controlled by equilibrated weight changes of the sample (dM/dT = 0.01% min^{-1}). Vacuum pressure transducers were used with ability to measure from 1×10^{-6} to 760 Torr with a resolution of 0.01%. Approximately 10 mg of sample was used for each experiment. The mass of the sample was determined by comparison to an empty reference pan and recorded by a high-resolution microbalance with a precision of 0.1 μg.

Dynamic CO_2 sorption study

Dynamic CO_2 sorption experiments were carried out using a Hiden Isochema XEMIS microbalance at 288 K. In each experiment, around 20 mg of sample (**sql-1-M-NCS**) was used and further evacuated *in situ* at 323 K for 5 h. Pressure was then maintained at 1 bar without pumping out until mass equilibrium was reached. The pressure was first elevated from 1 to 36 bar, held until mass equilibrium was reached, and then reduced from 36 to 1 bar with a maximum constant rate of 2.5 bar per min. Background calibration was applied by repeating the same procedure except that the **sql-1-M-NCS** sample was replaced by a 20 mg counterweight in the sample cell.

Author contributions

Shi-Qiang Wang: conceptualization, methodology, investigation, formal analysis, writing – original draft; Shaza Darwish: investigation, writing – review & editing; Debobroto Sensharma: investigation, writing – review & editing; Michael J. Zaworotko: supervision, funding acquisition, writing – review & editing.

Conflicts of interest

There are no conflicts to declare.

Acknowledgements

M. J. Z. would like to acknowledge the support of Irish Research Council (IRCLA/2019/167) and Science Foundation Ireland (13/RP/B2549 and 16/IA/4624). We thank Dr Claire Murray and Dr Chiu C. Tang at the Diamond Light Source, UK for the access to the synchrotron X-ray diffraction beamline i11 (EE20500). S.-Q. W. would also like to thank his colleagues, Mr Daniel O'Hearn, Dr Andrey Bezrukov and Dr Soumya Mukherjee, for their assistance at Diamond Light Source.

Notes and references

1 S. Kitagawa, *Angew. Chem., Int. Ed.*, 2015, **54**, 10686–10687.
2 C. M. Simon, J. Kim, D. A. Gomez-Gualdron, J. S. Camp, Y. G. Chung, R. L. Martin, R. Mercado, M. W. Deem, D. Gunter, M. Haranczyk, D. S. Sholl, R. Q. Snurr and B. Smit, *Energy Environ. Sci.*, 2015, **8**, 1190–1199.
3 M. Thommes, K. Kaneko, A. V. Neimark, J. P. Olivier, F. Rodriguez-Reinoso, J. Rouquerol and K. S. Sing, *Pure Appl. Chem.*, 2015, **87**, 1051–1069.
4 J. A. Mason, J. Oktawiec, M. K. Taylor, M. R. Hudson, J. Rodriguez, J. E. Bachman, M. I. Gonzalez, A. Cervellino,

Open Access Article. Published on 10 December 2021. Downloaded on 4/23/2024 8:59:29 PM. This article is licensed under a Creative Commons Attribution-NonCommercial 3.0 Unported Licence.

A. Guagliardi, C. M. Brown, P. L. Llewellyn, N. Masciocchi and J. R. Long, *Nature*, 2015, **527**, 357–361.
5 J. J. Perry IV, J. A. Perman and M. J. Zaworotko, *Chem. Soc. Rev.*, 2009, **38**, 1400–1417.
6 T. R. Cook, Y.-R. Zheng and P. J. Stang, *Chem. Rev.*, 2012, **113**, 734–777.
7 L. R. MacGillivray, *Metal-organic frameworks: design and application*, John Wiley & Sons, 2010.
8 D. Farrusseng, *Metal-organic frameworks: applications from catalysis to gas storage*, John Wiley & Sons, 2011.
9 S. Kitagawa, R. Kitaura and S. I. Noro, *Angew. Chem., Int. Ed.*, 2004, **43**, 2334–2375.
10 S. R. Batten, S. M. Neville and D. R. Turner, *Coordination polymers: design, analysis and application*, Royal Society of Chemistry, 2009.
11 C. Janiak and J. K. Vieth, *New J. Chem.*, 2010, **34**, 2366–2388.
12 D. J. O'Hearn, A. Bajpai and M. J. Zaworotko, *Small*, 2021, 2006351.
13 J.-R. Li, R. J. Kuppler and H.-C. Zhou, *Chem. Soc. Rev.*, 2009, **38**, 1477–1504.
14 B. Li, H.-M. Wen, Y. Cui, W. Zhou, G. Qian and B. Chen, *Adv. Mater.*, 2016, **28**, 8819–8860.
15 B. Moulton and M. J. Zaworotko, *Chem. Rev.*, 2001, **101**, 1629–1658.
16 N. W. Ockwig, O. Delgado-Friedrichs, M. O'Keeffe and O. M. Yaghi, *Acc. Chem. Res.*, 2005, **38**, 176–182.
17 P. Z. Moghadam, A. Li, X.-W. Liu, R. Bueno-Perez, S.-D. Wang, S. B. Wiggin, P. A. Wood and D. Fairen-Jimenez, *Chem. Sci.*, 2020, **11**, 8373–8387.
18 A. Schneemann, V. Bon, I. Schwedler, I. Senkovska, S. Kaskel and R. A. Fischer, *Chem. Soc. Rev.*, 2014, **43**, 6062–6096.
19 S. Horike, S. Shimomura and S. Kitagawa, *Nat. Chem.*, 2009, **1**, 695–704.
20 Q.-Y. Yang, P. Lama, S. Sen, M. Lusi, K. J. Chen, W. Y. Gao, M. Shivanna, T. Pham, N. Hosono, S. Kusaka, J. J. IV. Perry, S. Ma, B. Space, L. J. Barbour, S. Kitagawa and M. J. Zaworotko, *Angew. Chem., Int. Ed.*, 2018, **57**, 5684–5689.
21 S.-Q. Wang, S. Mukherjee and M. J. Zaworotko, *Faraday Discuss.*, 2021, **231**, 9–50.
22 S. Mukherjee and M. J. Zaworotko, *Trends Chem.*, 2020, **2**, 506–518.
23 J.-P. Zhang, H.-L. Zhou, D.-D. Zhou, P.-Q. Liao and X.-M. Chen, *Natl. Sci. Rev.*, 2018, **5**, 907–919.
24 S. K. Elsaidi, M. H. Mohamed, D. Banerjee and P. K. Thallapally, *Coord. Chem. Rev.*, 2018, **358**, 125–152.
25 S. Henke, A. Schneemann, A. Wuetscher and R. A. Fischer, *J. Am. Chem. Soc.*, 2012, **134**, 9464–9474.
26 A. Schneemann, P. Vervoorts, I. Hante, M. Tu, S. Wannapaiboon, C. Sternemann, M. Paulus, D. C. F. Wieland, S. Henke and R. A. Fischer, *Chem. Mater.*, 2018, **30**, 1667–1676.
27 N. A. Ramsahye, T.-K. Trung, S. Bourrelly, Q.-Y. Yang, T. Devic, G. Maurin, P. Horcajada, P. L. Llewellyn, P. Yot, C. Serre, Y. Filinchuk, F. Fajula, G. Ferey and P. Trens, *J. Phys. Chem. C*, 2011, **115**, 18683–18695.
28 T. Devic, F. Salles, S. Bourrelly, B. Moulin, G. Maurin, P. Horcajada, C. Serre, A. Vimont, J.-C. Lavalley, H. Leclerc, G. Clet, M. Daturi, P. L. Llewellyn, Y. Filinchuk and G. Ferey, *J. Mater. Chem.*, 2012, **22**, 10266–10273.
29 M. K. Taylor, T. Runčevski, J. Oktawiec, M. I. Gonzalez, R. L. Siegelman, J. A. Mason, J. Ye, C. M. Brown and J. R. Long, *J. Am. Chem. Soc.*, 2016, **138**, 15019–15026.
30 A.-X. Zhu, Q.-Y. Yang, A. Kumar, C. Crowley, S. Mukherjee, K.-J. Chen, S.-Q. Wang, D. O'Nolan, M. Shivanna and M. J. Zaworotko, *J. Am. Chem. Soc.*, 2018, **140**, 15572–15576.
31 A.-X. Zhu, Q.-Y. Yang, S. Mukherjee, A. Kumar, C.-H. Deng, A. A. Bezrukov, M. Shivanna and M. J. Zaworotko, *Angew. Chem., Int. Ed.*, 2019, **58**, 18212–18217.
32 S. Bourrelly, P. L. Llewellyn, C. Serre, F. Millange, T. Loiseau and G. Férey, *J. Am. Chem. Soc.*, 2005, **127**, 13519–13521.
33 P. L. Llewellyn, P. Horcajada, G. Maurin, T. Devic, N. Rosenbach, S. Bourrelly, C. Serre, D. Vincent, S. Loera-Serna, Y. Filinchuk and G. Ferey, *J. Am. Chem. Soc.*, 2009, **131**, 13002–13008.
34 J. P. Mowat, V. R. Seymour, J. M. Griffin, S. P. Thompson, A. M. Slawin, D. Fairen-Jimenez, T. Düren, S. E. Ashbrook and P. A. Wright, *Dalton Trans.*, 2012, **41**, 3937–3941.
35 S. Galli, N. Masciocchi, V. Colombo, A. Maspero, G. Palmisano, F. J. López-Garzón, M. Domingo-García, I. Fernández-Morales, E. Barea and J. A. R. Navarro, *Chem. Mater.*, 2010, **22**, 1664–1672.
36 N. Klein, H. C. Hoffmann, A. Cadiau, J. Getzschmann, M. R. Lohe, S. Paasch, T. Heydenreich, K. Adil, I. Senkovska, E. Brunner and K. Stefan, *J. Mater. Chem.*, 2012, **22**, 10303–10312.
37 C. M. McGuirk, T. Runčevski, J. Oktawiec, A. Turkiewicz, M. K. Taylor and J. R. Long, *J. Am. Chem. Soc.*, 2018, **140**, 15924–15933.
38 T. G. Mitina and V. A. Blatov, *Cryst. Growth Des.*, 2013, **13**, 1655–1664.
39 M. J. Zaworotko, *Chem. Commun.*, 2001, 1–9.
40 M. Fujita, Y. J. Kwon, S. Washizu and K. Ogura, *J. Am. Chem. Soc.*, 1994, **116**, 1151–1152.
41 D. Li and K. Kaneko, *Chem. Phys. Lett.*, 2001, **335**, 50–56.
42 A. Kondo, H. Noguchi, S. Ohnishi, H. Kajiro, A. Tohdoh, Y. Hattori, W.-C. Xu, H. Tanaka, H. Kanoh and K. Kaneko, *Nano Lett.*, 2006, **6**, 2581–2584.
43 H. Kanoh, A. Kondo, H. Noguchi, H. Kajiro, A. Tohdoh, Y. Hattori, W.-C. Xu, M. Inoue, T. Sugiura, K. Morita, H. Tanaka, T. Ohba and K. Kaneko, *J. Colloid Interface Sci.*, 2009, **334**, 1–7.
44 H. Kajiro, A. Kondo, K. Kaneko and H. Kanoh, *Int. J. Mol. Sci.*, 2010, **11**, 3803–3845.
45 V. Bon, I. Senkovska, D. Wallacher, A. Heerwig, N. Klein, I. Zizak, R. Feyerherm, E. Dudzik and S. Kaskel, *Microporous Mesoporous Mater.*, 2014, **188**, 190–195.
46 L. Li, R. Krishna, Y. Wang, X. Wang, J. Yang and J. Li, *Eur. J. Inorg. Chem.*, 2016, 4457–4462.
47 S.-Q. Wang, X.-Q. Meng, M. Vandichel, S. Darwish, Z. Chang, X.-H. Bu and M. J. Zaworotko, *ACS Appl. Mater. Interfaces*, 2021, **13**, 23877–23883.
48 A. Kondo, A. Chinen, H. Kajiro, T. Nakagawa, K. Kato, M. Takata, Y. Hattori, F. Okino, T. Ohba, K. Kaneko and H. Kanoh, *Chem. – Eur. J.*, 2009, **15**, 7549–7553.

© 2022 The Author(s). Published by the Royal Society of Chemistry

Open Access Article. Published on 10 December 2021. Downloaded on 4/23/2024 8:59:29 PM.
This article is licensed under a Creative Commons Attribution-NonCommercial 3.0 Unported Licence.

49 J. Lu, T. Paliwala, S. C. Lim, C. Yu, T. Y. Niu and A. J. Jacobson, *Inorg. Chem.*, 1997, **36**, 923–929.
50 S.-Q. Wang, Q.-Y. Yang, S. Mukherjee, D. O'Nolan, E. Patyk-Kaźmierczak, K.-J. Chen, M. Shivanna, C. Murray, C. C. Tang and M. J. Zaworotko, *Chem. Commun.*, 2018, **54**, 7042–7045.
51 S.-Q. Wang, S. Mukherjee, E. Patyk-Kaźmierczak, S. Darwish, A. Bajpai, Q.-Y. Yang and M. Zaworotko, *Angew. Chem., Int. Ed.*, 2019, **58**, 6630–6634.
52 Z. Yugen, J. Li, W. Deng, N. Masayoshi and I. Tsuneo, *Chem. Lett.*, 1999, 195–196.
53 H. Irving and R. J. P. Williams, *J. Chem. Soc.*, 1953, 3192–3210.
54 M. Ichikawa, A. Kondo, H. Noguchi, N. Kojima, T. Ohba, H. Kajiro, Y. Hattori and H. Kanoh, *Langmuir*, 2016, **32**, 9722–9726.
55 S. Hiraide, H. Tanaka, N. Ishikawa and M. T. Miyahara, *ACS Appl. Mater. Interfaces*, 2017, **9**, 41066–41077.
56 Y. Wang and D. Zhao, *Cryst. Growth Des.*, 2017, **17**, 2291–2308.
57 P. Nugent, Y. Belmabkhout, S. D. Burd, A. J. Cairns, R. Luebke, K. Forrest, T. Pham, S. Q. Ma, B. Space, L. Wojtas, M. Eddaoudi and M. J. Zaworotko, *Nature*, 2013, **495**, 80–84.
58 K. Li, D. H. Olson, J. Seidel, T. J. Emge, H. Gong, H. Zeng and J. Li, *J. Am. Chem. Soc.*, 2009, **131**, 10368–10369.
59 D. Tanaka, K. Nakagawa, M. Higuchi, S. Horike, Y. Kubota, T. C. Kobayashi, M. Takata and S. Kitagawa, *Angew. Chem., Int. Ed.*, 2008, **47**, 3914–3918.
60 A. M. Kałuża, S. Mukherjee, S.-Q. Wang, D. J. O'Hearn and M. J. Zaworotko, *Chem. Commun.*, 2020, **56**, 1940–1943.
61 F. Millange, C. Serre, N. Guillou, G. Ferey and R. I. Walton, *Angew. Chem., Int. Ed.*, 2008, **47**, 4100–4105.
62 S. Choi, J. H. Drese and C. W. Jones, *ChemSusChem*, 2009, **2**, 796–854.
63 P. Wang, T. Kajiwara, K.-I. Otake, M.-S. Yao, H. Ashitani, Y. Kubota and S. Kitagawa, *ACS Appl. Mater. Interfaces*, 2021, **13**, 52144–52151.
64 M.-H. Yu, B. Space, D. Franz, W. Zhou, C. He, L. Li, R. Krishna, Z. Chang, W. Li, T.-L. Hu and X.-H. Bu, *J. Am. Chem. Soc.*, 2019, **141**, 17703–17712.
65 Y. He, W. Zhou and B. Chen. *Current Status of Porous Metal-Organic Frameworks for Methane Storage*, Metal–Organic Frameworks: Applications in Separations and Catalysis Wiley-VCH, 2018, pp. 163–198.